






## Article

# Evaluation of Sinusoidal Distribution Networks Using the EPC Simulation Software

Vicente León-Martínez <sup>1</sup>, Joaquín Montañana-Romeu <sup>1,\*</sup>, Elisa Peñalvo-López <sup>1</sup>, Manuel A. Graña-López <sup>2</sup>  
and Ivan Valencia-Salazar <sup>1</sup>

<sup>1</sup> Electrical Engineering Department, Universitat Politècnica de València, 46022 València, Spain

<sup>2</sup> Industrial Engineering Department, Universidade A Coruña, 15071 A Coruña, Spain

\* Correspondence: jmontanana@die.upv.es

**Abstract:** The electric power calculator (EPC) software, for the simulation and analysis of electrical networks at the industrial frequency, is described in this article, including its source code and operational diagram. Compared to well-known commercial software, EPC directly provides the values of the voltages, currents, and powers in each subsystem. The voltages and currents are calculated, in phasor notation, applying Kirchhoff's laws, while the powers are obtained through the components of the apparent power vector. In this paper, the EPC software could be applied to three-phase networks made up of a distribution transformer and two three-phase wye-configured loads. The correctness of the results of the EPC software was verified by comparison with those obtained using the Multisim commercial software and with the measurements recorded by the Fluke 435 analyzer in a real distribution network of residential buildings. The values of the voltages and currents provided by the EPC were the same as those measured by the Fluke, and the differences observed using Multisim were less than 0.6%. Consequently, the EPC software is an excellent complement for power analyzers, because it is capable of providing measurements in all the network subsystems at the same time, using a single analyzer.

**Keywords:** building networks; distribution systems; simulation software; power measurement; industrial frequency



**Citation:** León-Martínez, V.; Montañana-Romeu, J.;

Peñalvo-López, E.; Graña-López, M.A.; Valencia-Salazar, I. Evaluation of Sinusoidal Distribution Networks Using the EPC Simulation Software. *Buildings* **2023**, *13*, 716. <https://doi.org/10.3390/buildings13030716>

Academic Editors: Wei Liu, Jan Košny and Benedetto Nastasi

Received: 10 January 2023

Revised: 1 February 2023

Accepted: 6 March 2023

Published: 8 March 2023



**Copyright:** © 2023 by the authors. Licensee MDPI, Basel, Switzerland. This article is an open access article distributed under the terms and conditions of the Creative Commons Attribution (CC BY) license (<https://creativecommons.org/licenses/by/4.0/>).

## 1. Introduction

Engineers and technicians need to know the state of operation of the electrical networks in their charge, as well as evaluate, in advance, the effects of non-useful energy and those produced by untimely defects. The analysis of the operation of the electrical networks in a steady state can be carried out using either of the two following procedures: (1) carrying out measurements in situ, with measuring instruments, or (2) using simulation software. The first procedure has the advantage of providing accurate results, although it requires the use of network analyzers installed in the different subsystems of the network during the study period. The second procedure makes the following possible:

- To obtain measurements in all the subsystems at the same time, without the need to use numerous and expensive measuring devices;
- To analyze the operation of electrical networks by applying efficiency improvement techniques (compensation for reactive power and imbalances);
- To simulate operation in dangerous scenarios as practice (such as the presence of short circuits or accidental breakage of the neutral conductor, among other possible study cases).

The technical literature includes abundant examples of analysis software of electrical and electronic circuits, both open-source and commercial. Of the software analyzed, the following stand out, in our opinion: Multisim, LTSpice, Proteus, and PSCAD. All of these

can be run using the Windows 10 operating system; the first three are based on the SPICE simulator, while PSCAD uses EMT (electromagnetic transients) as a simulation engine.

Multisim [1], from National Instruments, has an interactive environment with electrical schematics, which allows instant visualization and analysis of the operation of electrical circuits, as well as transfer of the results obtained after the simulation to LabVIEW analysis software. LTSpice [2], from the analog chip company Linear Technology, has a graphical interface to test analog circuit diagrams and obtain simulation results, and its waveforms can be viewed through a built-in viewer. Proteus [3], from LabCenter, is a circuit simulation software, which includes elements such as measuring devices, signal generators, switches, and lamps, among others. In addition, it includes visualizing graphs of basic functions (frequency, distortion, noise, etc.) obtained from the measurements of voltages and currents. PSCAD [4], developed by the Engineering and Development department of the Canadian company Manitoba Hydro International Ltd. (MHI), is a power system simulation software that works with mathematical models (Newton–Raphson, Runge–Kutta). It has a very extensive library, which includes everything from simple elements to electrical machines. These tools are useful for calculating the voltages and currents of electrical and electronic circuits, although, in many of them, obtaining the values of these quantities must be complemented by the use of LabVIEW 2015 analysis software.

The electric power calculator simulation software, described in this paper, allows the direct calculation, without the additional use of LabVIEW software, of the voltages and currents in the different subsystems of sinusoidal three-phase networks and the visualization of their values on the “system voltages and currents” screen. In the version described in the paper, the EPC software was developed using the Excel platform (although it could also be carried out with LabVIEW). Likewise, this EPC version can be applied to wye-configured three-phase circuits, such as the one represented in Figure 1, which is formed by a transformer. The secondary configuration is a star, and two three-phase loads are also configured as a star, with a neutral conductor.

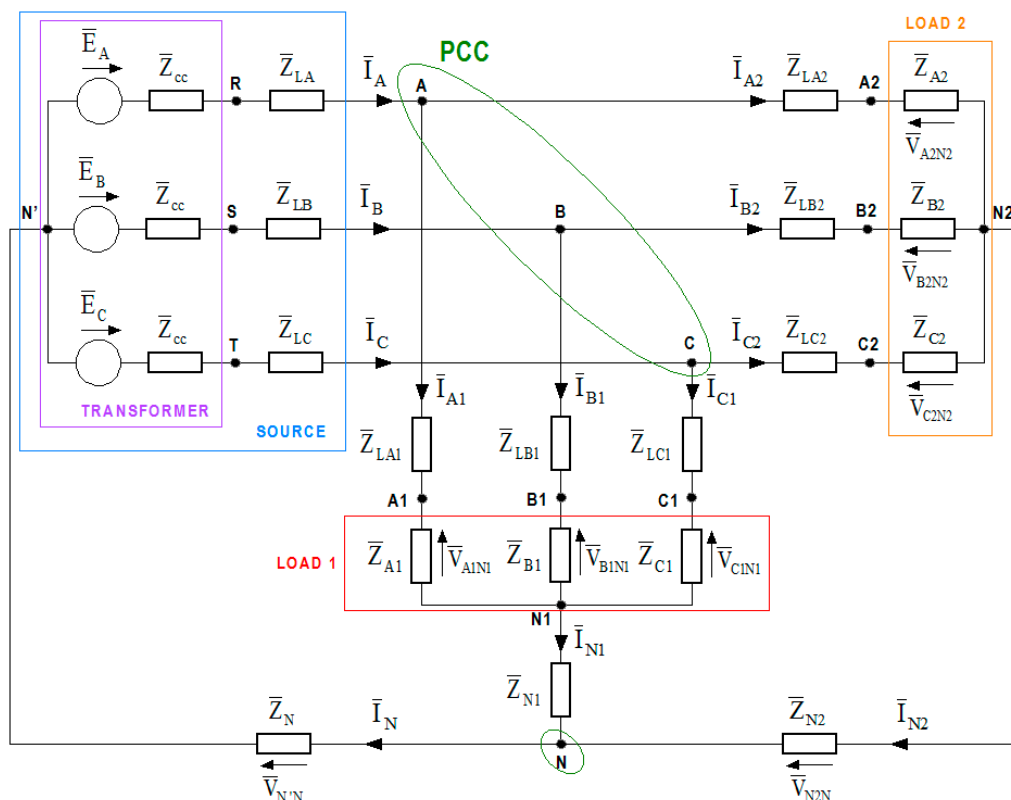


Figure 1. Schematic representation of the three-phase system and its different subsystems.

In the three-phase system of Figure 1, five subsystems can be distinguished:

(1) The transformer (TRANSFORMER); (2) the source (SOURCE), formed by the transformer and the main line, with neutral point  $N'$ ; (3) the point of common coupling (PCC), which is the connection point of the source and loads, with neutral point  $N$ ; (4) the first load (LOAD 1), made up of that load and its individual line; and (5) the second load (LOAD 2), made up of that load and its individual line.

Alike, the EPC software provides the values of the apparent powers and their components (positive-sequence active and reactive, and unbalanced powers), in addition to the active and reactive powers. These powers are obtained in each of the subsystems and are displayed on the “apparent powers and components” screen. As a novelty, compared to other simulation software, EPC uses vector expressions to determine the apparent and unbalanced powers, which were developed in [5]. The module of the apparent power vector always coincides with the value of Buchholz’s apparent power [6]. The use of these powers in vector notation gives great potential to the EPC software to simulate operations with unbalanced loads, as seen in [5], and even to analyze the integration of renewable energies in distribution networks. The study of the operation of unbalanced electrical networks is of great interest [7–20], and the components of the unbalanced power vector ( $\vec{S}_u$ ) allow us to separately analyze the power effects of imbalances according to each of their causes, namely, imbalances in active power supplies, imbalances in reactive power supplies, and imbalances in supply voltages.

Additionally, the EPC software supplies the values of the neutral-displacement power ( $S_n$ ) [21] and its relationship with the apparent power ( $S_n/S$ ). The last parameter determines the effect of the operation of the neutral conductor in each subsystem. Equally, the EPC software provides the values of the apparent powers according to the IEEE 1459–2010 [22] and DIN 40110-2 [23] standards, at the point of common coupling (PCC) of the three-phase system shown in Figure 1.

The EPC software screens used for entering data and reading the calculated voltages, currents, and powers are described in Section 2. The diagrams and operating equations, which constitute the source code of the EPC software, are established in Section 3. In Section 4 of this article, the EPC software is used on a real distribution network supplying residential buildings as an application example, and its results are compared with the measures recorded by the power analyzer Fluke 435 Series II, as well as with those values obtained with the commercial software Multisim. Finally, the conclusions are presented in Section 5.

## 2. EPC Software Screens

The EPC software has three screens: “system data”, “apparent powers and components”, and “system voltages, and currents”, which include the data values and results in each of the subsystems represented in Figure 1.

### 2.1. “System Data” Screen

The first step in using the EPC software is to enter the characteristic values (features) of the transformer, loads, lines, and neutral conductors on the “system data” screen (Figure 2).

On this screen, it can be seen that each subsystem has its corresponding table or tables, with its cells being initially empty, to enter the characteristic values of each subsystem. It is important to note that it is necessary to fill in all the cells of these tables for the correct operation of the software. If any cell must have an infinite value, it is enough to include a very high value, greater than  $10^6$ , for example, while, if there must be a value equal to zero in a cell, it is enough to enter a value of at least  $10^{-6}$  for the software to work correctly.

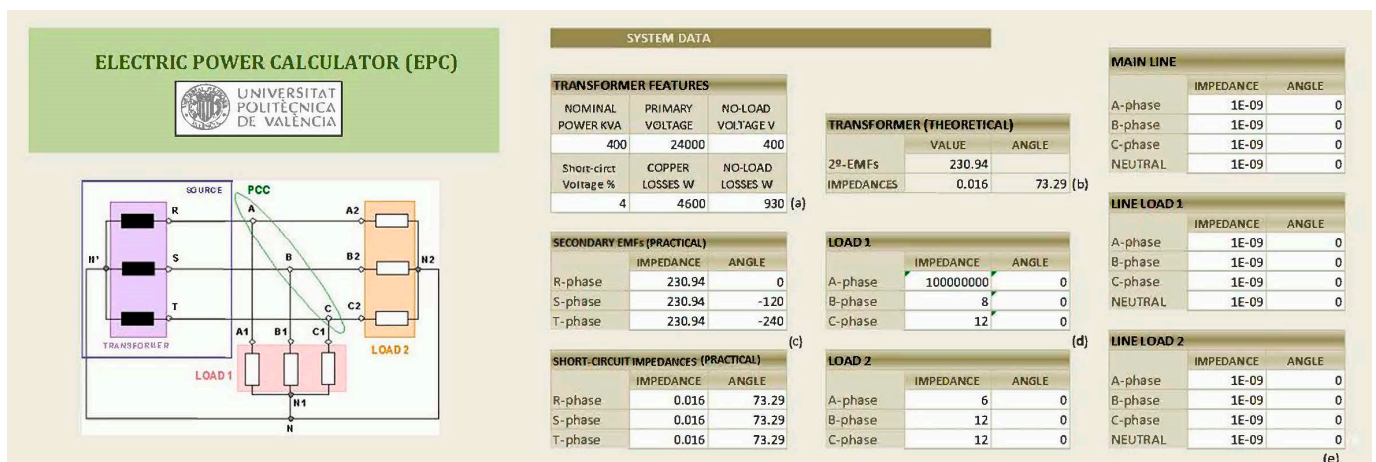


**Figure 2.** “System data” screen: (a) transformer features; (b) theoretical values of transformer secondary EMFs and short-circuit impedances; (c) practical values of secondary EMFs and short-circuit impedances; (d) load impedances; and (e) line and neutral conductor impedances.

- Table of transformer features (Figure 2a).

The table for entering the of transformer features has six boxes, in which the user must enter the following transformer data:

- Nominal power, in kilovolt–Amperes (kVA).
- Primary voltage, in volts (V).
- No-load secondary voltage, in volts (V).
- Short-circuit voltage, in percent (%).
- Copper losses, in watts (W).
- No-load losses, in watts (W).

With these values, the software calculates the phasors of the secondary EMFs and the transformer short-circuit impedances, as presented in the table of Figure 2b. The user of the EPC software has the possibility of directly using these theoretical values and entering them in the tables of Figure 2c, or else modifying these values in each phase to adjust them to the constructive asymmetries of the transformer.

- Tables of three-phase load complex impedances (Figure 2d).

The values of the module and the angle of the complex impedances of each phase of the loads (named LOAD 1 and LOAD 2) must be entered in the cells of two tables (Figure 2d). The module of these impedances is entered in ohms ( $\Omega$ ) and their angles are in degrees (not radians).

Note that if there is only one three-phase load or there are single-phase loads, no empty cells should be left in the load tables. The software correctly operates when the modules of the impedances of the non-existent phases are filled with a very high value, greater than  $10^6$ . The assigned angles of the non-existent impedances can have any value, but these cells must always be filled in.

- Tables of line complex impedances (Figure 2e).

The values of the module, in ohms ( $\Omega$ ), and the angle, in degrees ( $^\circ$ ), of the line and neutral conductor complex impedances are entered in the cells of three tables (Figure 2e).

In the system of Figure 1, there are three lines, which connect the secondary line of the transformer with the loads. The MAIN LINE connects the secondary line of the transformer with the point of common coupling (PCC) with the loads. The taps to each load connect the PCC with the first load (LINE LOAD 1) and with the second load (LINE LOAD 2), respectively.

Note that all cells must be filled in. If any line or any phase of a line does not exist, either because it does not feed any load or due to accidental breakage, the cells of the

impedance modules of these lines will be filled with a very high value, greater than  $10^6$ , while any value can fill the cells of the angles.

The complex impedances of the phases and the neutral conductor of each line can have different values. In this way, it is possible to simulate different lengths and sections of the conductor, as well as the breaking process of one phase of the line or the neutral conductor, progressively increasing their values.

## 2.2. Screen of “Apparent Powers and Components”

This screen (Figure 3) summarizes, in tables, the values of the modules of the apparent power vector, the unbalanced power vector, and its components. Furthermore, it summarizes the value of the neutral-displacement power, calculated by the EPC software at the industrial frequency, for each one of the subsystems of the sinusoidal three-phase system represented in Figure 1. In addition, this screen indicates the values of apparent power calculated in the common point of coupling (PCC) according to IEEE 1459-2010 and DIN 40110-2 standards. For each subsystem, there are three tables (Figure 4) named “apparent powers and components”, “unbalanced powers and components”, and “neutral-displacement power”.

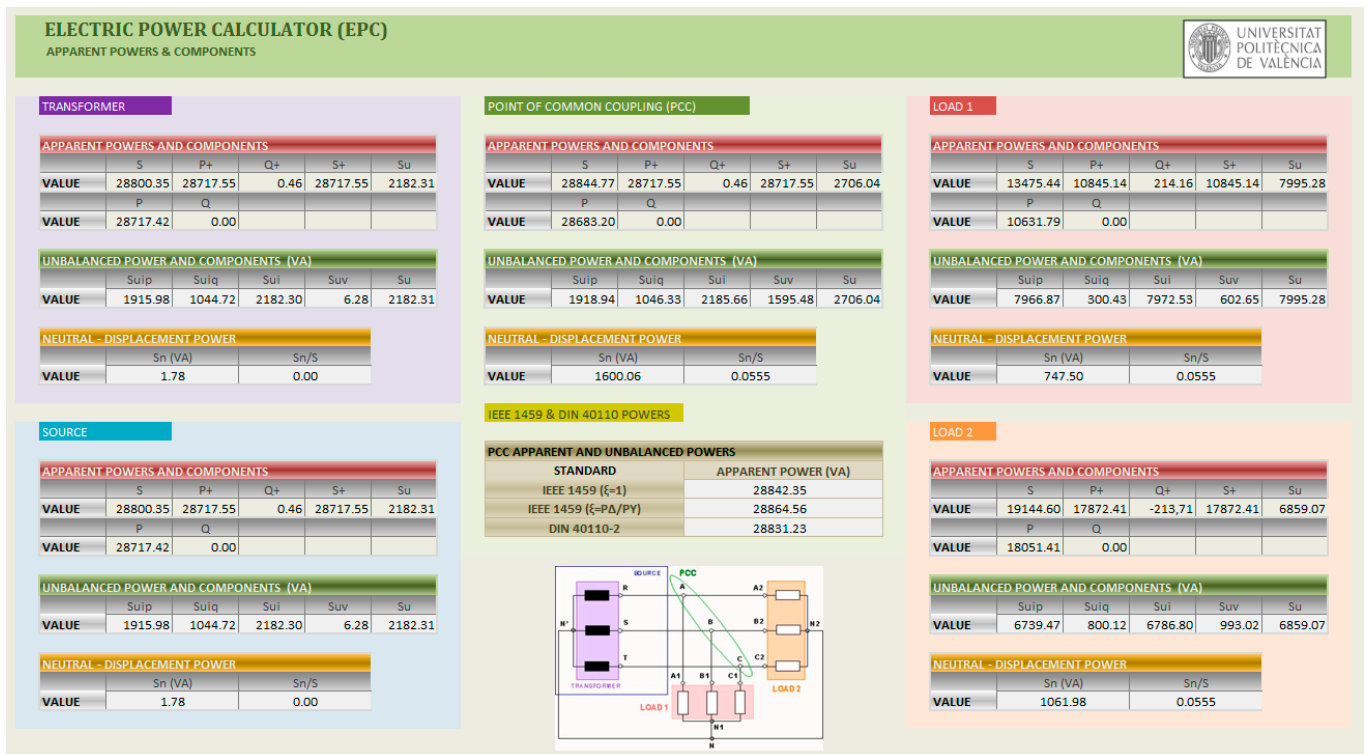


Figure 3. Screen of “Apparent Powers and Components”.

The table of “apparent power and components” shows the module values of the apparent power vector ( $S$ ) of each subsystem in VA and its components, namely, the positive-sequence active power ( $P_+$ ), in W, the positive-sequence reactive power ( $Q_+$ ), in var, and the unbalanced power ( $S_u$ ), in VA. Likewise, this table includes the values of the positive-sequence apparent power ( $S_+$ ), in VA, of the active power ( $P$ ), in W, and of the reactive power ( $Q$ ), in var, calculated in each subsystem.

The table of “unbalanced powers and components” summarizes the module values of the unbalanced power vector ( $S_u$ ) in each subsystem in VA and its components, namely, those due to active power ( $S_{uip}$ ) and reactive power ( $S_{uiq}$ ) imbalances;  $S_{ui}$ , which measures the combined effects of  $S_{uip}$  and  $S_{uiq}$ ; and  $S_{uv}$ , which measures the effects of the voltage imbalances.



The table of “neutral-displacement power” shows the neutral-displacement power values ( $S_n$ ), which determine the effects of the operation of the neutral conductor in each subsystem in VA. Evenly, these tables include the relative values of the ratio between the neutral-displacement power and the apparent power ( $S_n/S$ ) in each subsystem. This relative value is higher according to the deterioration of the neutral conductor increases.

Likewise, the “apparent powers and components” screen also includes a table with the values of the apparent powers calculated in the PCC according to the IEEE 1459-2010 and DIN 40110-2 standards. The apparent powers according to the IEEE 1459-2010 standard are calculated for two values of the parameter  $\zeta$ , defined by this standard as the quotient between the active power of the delta and star loads ( $\zeta = P_\Delta/P_Y$ ). The value  $\zeta = 0$  corresponds to the electrical system of Figure 1, in which there are no delta loads. The value  $\zeta = 1$  is recommended by the standard if the values of  $P_\Delta$  and  $P_Y$  are unknown.

### 2.3. Screen of “System Voltages and Currents”

This screen summarizes the phasor values of the voltages and currents calculated by the EPC software in the phases of each subsystem (Figure 4).

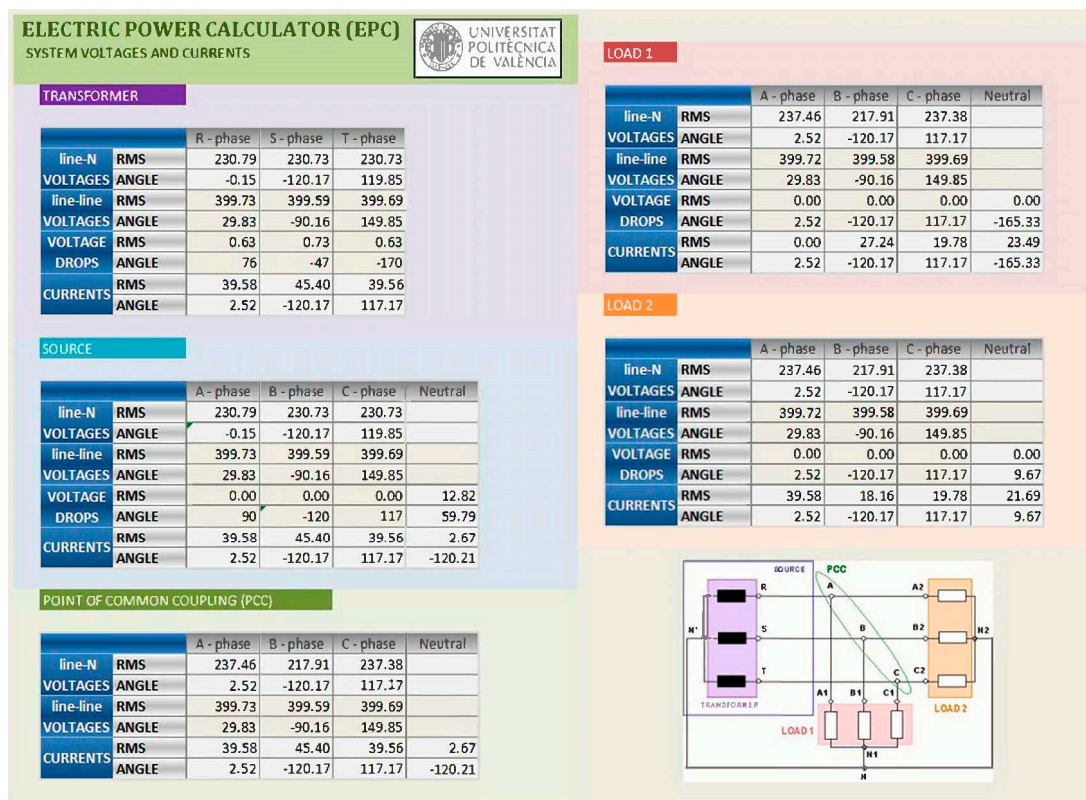


Figure 4. Screen of “System Voltages and Currents”.

The tables corresponding to the source, load 1, and load 2 show the phasors (RMS value and angle) of the following quantities for each of these subsystems (Figure 5):

- Line-to-neutral voltages, in volts (V).
- Line-to-line voltages, in volts (V).
- Line and neutral voltage drops, in volts (V).

Line and neutral currents, in amperes (A).

The line-to-neutral transformer and source voltages are calculated on the neutral point of the transformer ( $N'$ ), while the line-to-neutral PCC and load voltages are measured on the neutral point of each of these subsystems ( $N$ ,  $N1$ , and  $N2$ , respectively).

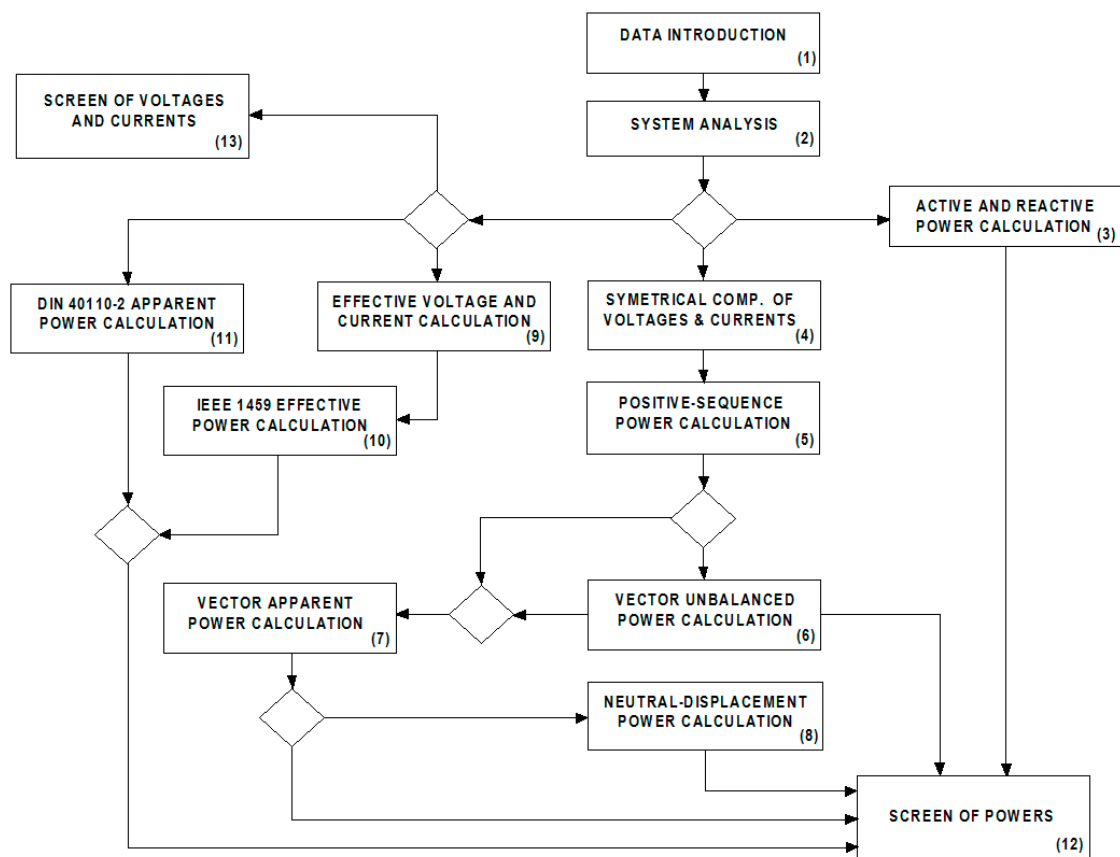


Figure 5. Operational diagram of the EPC software.

### 3. Description of the EPC Software

This section describes the operational diagram of the software “electric power calculator” (EPC) and establishes the equations that make up its source code.

#### 3.1. Operational Diagram

The operational sequence of the EPC software is represented in Figure 5. It begins with the manual input of the data, in (1), and the analysis of the system represented in Figure 1, in (2), which determines the values of the voltages and currents in its different subsystems by application of Ohm’s law and Kirchhoff’s laws. With these voltages and currents, in (3), the active and reactive powers in each subsystem are obtained. The application of Fortescue’s theorem [24] determines, in (4), the positive-sequence components of the voltages and currents in the different subsystems, from which the positive-sequence active, reactive, and apparent powers are obtained, in (5), and the unbalanced powers in (6). The apparent power vector and its components are obtained, in (7), from the positive-sequence powers and the unbalanced power vector [5]. The neutral-displacement power is determined, in (8), according to [21]. Equally, from the values of the voltages and currents in the different subsystems, obtained in (2), the effective voltages and currents are determined, in (9), according to the IEEE Standard 1459-2010 [23], and the effective apparent powers in (10). The apparent powers according to DIN 40110-2 [24] are calculated, in (11), based on the voltages and currents determined in (2). These powers are displayed on the “Apparent Powers and Components” screen in (12).

Voltages and currents, calculated in (2) for the different subsystems, are shown on the screen of “System Voltages and Currents” in (13).

### 3.2. Source Code

The “electric power calculator” (EPC) software has been developed in two blocks or programming modules. The first and main module, designated as the power module, in which the values of the apparent power vector, unbalanced power vector, and neutral-displacement power, is determined. The second, we named the voltage and current module, in which the values of the voltages and currents in each subsystem, necessary for the power calculation, is obtained.

#### 3.2.1. Power Programming Module

This module (Figure 6) is used for determining the apparent power vector and its components in each subsystem, at the industrial frequency, based on the values of the voltages and currents obtained in the different subsystems. This is carried out after entering data in stage (1) and after the analysis of the system in stage (2) of this programming module.

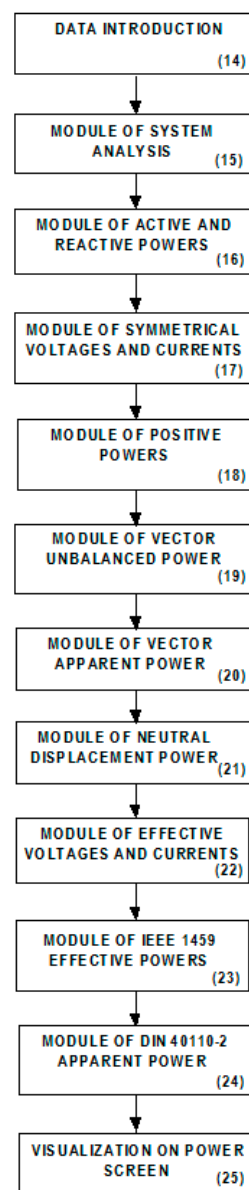


Figure 6. Power programming module.

The power programming module comprises the following stages:



- (a) Data entry in stage (14) of the programming module. In this stage, the characteristic values of the transformer, of the lines, and of the neutral conductors, as well as of the load phases of the system of Figure 1, are incorporated. With the entered values, we know:

- the complex impedances of the first load ( $\bar{Z}_{A1}, \bar{Z}_{B1}, \bar{Z}_{C1}$ ), the complex impedances of the second load ( $\bar{Z}_{A2}, \bar{Z}_{B2}, \bar{Z}_{C2}$ ), the complex impedances of the main line ( $\bar{Z}_{LA}, \bar{Z}_{LB}, \bar{Z}_{LC}$  and  $\bar{Z}_n$ ), and the complex impedances of the lines of the first load ( $\bar{Z}_{LA1}, \bar{Z}_{LB1}, \bar{Z}_{LC1}$  and  $\bar{Z}_{n1}$ ) and of the lines of the second load ( $\bar{Z}_{LA2}, \bar{Z}_{LB2}, \bar{Z}_{LC2}$  and  $\bar{Z}_{n2}$ );
- the theoretical phasors of the secondary EMFs of the transformer ( $\bar{E}_A, \bar{E}_B, \bar{E}_C$ ),

$$\bar{E}_A = \frac{V_{20}}{\sqrt{3}} \angle 0^\circ \quad \bar{E}_B = \bar{E}_A \angle -120^\circ \quad \bar{E}_C = \bar{E}_A \angle 120^\circ \quad (1)$$

where  $V_{20}$  is the no-load secondary line-to-line voltage;

- the module ( $Z_{cc}$ ) and the angle ( $\varphi_{cc}$ ) of the short-circuit impedances of the transformer,

$$Z_{cc} = \frac{V_{20}^2 \cdot \varepsilon\%}{100 \cdot S_N} \quad \varphi_{cc} = \text{inv} \cos \frac{100 \cdot P_{JN}}{\varepsilon\% \cdot S_N} \quad (2)$$

where  $S_N$  is the rated power of the transformer,  $\varepsilon\%$  is the rated short-circuit voltage (in %), and  $P_{JN}$  is the rated copper losses.

- (b) Analysis of the system in stage (15) of the programming module. This stage includes the calculation of the phase voltages and currents of the different subsystems. To do this, the analysis method of node voltages is applied to the system represented in Figure 1, using the node N, corresponding to the neutral point of the PCC, as the voltage reference, obtaining the following equations:

- Node A (PCC):

$$\frac{\bar{E}_A}{\bar{Z}_{cc} + \bar{Z}_{LA}} = \left( \frac{1}{\bar{Z}_{cc} + \bar{Z}_{LA}} + \frac{1}{\bar{Z}_{LA1} + \bar{Z}_{A1}} + \frac{1}{\bar{Z}_{LA2} + \bar{Z}_{A2}} \right) \cdot \bar{V}_{AN} - \frac{1}{\bar{Z}_{LA1} + \bar{Z}_{A1}} \bar{V}_{N1N} - \frac{1}{\bar{Z}_{LA2} + \bar{Z}_{A2}} \bar{V}_{N2N} - \frac{1}{\bar{Z}_{cc} + \bar{Z}_{LA}} \bar{V}_{N'N} \quad (3)$$

- Node B (PCC):

$$\frac{\bar{E}_B}{\bar{Z}_{cc} + \bar{Z}_{LB}} = \left( \frac{1}{\bar{Z}_{cc} + \bar{Z}_{LB}} + \frac{1}{\bar{Z}_{LB1} + \bar{Z}_{B1}} + \frac{1}{\bar{Z}_{LB2} + \bar{Z}_{B2}} \right) \cdot \bar{V}_{BN} - \frac{1}{\bar{Z}_{LB1} + \bar{Z}_{B1}} \bar{V}_{N1N} - \frac{1}{\bar{Z}_{LB2} + \bar{Z}_{B2}} \bar{V}_{N2N} - \frac{1}{\bar{Z}_{cc} + \bar{Z}_{LB}} \bar{V}_{N'N} \quad (4)$$

- Node C (PCC):

$$\frac{\bar{E}_C}{\bar{Z}_{cc} + \bar{Z}_{LC}} = \left( \frac{1}{\bar{Z}_{cc} + \bar{Z}_{LC}} + \frac{1}{\bar{Z}_{LC1} + \bar{Z}_{C1}} + \frac{1}{\bar{Z}_{LC2} + \bar{Z}_{C2}} \right) \cdot \bar{V}_{CN} - \frac{1}{\bar{Z}_{LC1} + \bar{Z}_{C1}} \bar{V}_{N1N} - \frac{1}{\bar{Z}_{LC2} + \bar{Z}_{C2}} \bar{V}_{N2N} - \frac{1}{\bar{Z}_{cc} + \bar{Z}_{LC}} \bar{V}_{N'N} \quad (5)$$

- Node N1 (neutral point of load 1):

$$0 = \left( \frac{1}{\bar{Z}_{LA1} + \bar{Z}_{A1}} + \frac{1}{\bar{Z}_{LB1} + \bar{Z}_{B1}} + \frac{1}{\bar{Z}_{LC1} + \bar{Z}_{C1}} + \frac{1}{\bar{Z}_{n1}} \right) \cdot \bar{V}_{N1N} - \frac{1}{\bar{Z}_{LA1} + \bar{Z}_{A1}} \bar{V}_{AN} - \frac{1}{\bar{Z}_{LB1} + \bar{Z}_{B1}} \bar{V}_{BN} - \frac{1}{\bar{Z}_{LC1} + \bar{Z}_{C1}} \bar{V}_{CN} \quad (6)$$

- Node N2 (neutral point of load 2):

$$0 = \left( \frac{1}{\bar{Z}_{LA2} + \bar{Z}_{A2}} + \frac{1}{\bar{Z}_{LB2} + \bar{Z}_{B2}} + \frac{1}{\bar{Z}_{LC2} + \bar{Z}_{C2}} + \frac{1}{\bar{Z}_{n2}} \right) \cdot \bar{V}_{N2N} - \frac{1}{\bar{Z}_{LA2} + \bar{Z}_{A2}} \bar{V}_{AN} - \frac{1}{\bar{Z}_{LB2} + \bar{Z}_{B2}} \bar{V}_{BN} - \frac{1}{\bar{Z}_{LC2} + \bar{Z}_{C2}} \bar{V}_{CN} \quad (7)$$

- Node N' (neutral point of the transformer):

$$\begin{aligned}
-\frac{\bar{E}_A}{\bar{Z}_{cc} + \bar{Z}_{LA}} - \frac{\bar{E}_B}{\bar{Z}_{cc} + \bar{Z}_{LB}} - \frac{\bar{E}_C}{\bar{Z}_{cc} + \bar{Z}_{LC}} &= \left( \frac{1}{\bar{Z}_{cc} + \bar{Z}_{LA}} + \frac{1}{\bar{Z}_{cc} + \bar{Z}_{LB}} + \frac{1}{\bar{Z}_{cc} + \bar{Z}_{LC}} \right) \cdot \bar{V}_{N'N} - \frac{1}{\bar{Z}_{cc} + \bar{Z}_{LA}} \bar{V}_{AN} - \\
&- \frac{1}{\bar{Z}_{cc} + \bar{Z}_{LB}} \bar{V}_{BN} - \frac{1}{\bar{Z}_{cc} + \bar{Z}_{LC}} \bar{V}_{CN}
\end{aligned} \quad (8)$$

The unknowns in these equations are the PCC line-to-neutral voltages ( $\bar{V}_{AN}$ ,  $\bar{V}_{BN}$ ,  $\bar{V}_{CN}$ ) and the voltage differences between the neutral points of the transformer ( $\bar{V}_{N'N}$ ), of the first load ( $\bar{V}_{N1N}$ ) the second load ( $\bar{V}_{N2N}$ ), and the PCC neutral point ( $N$ ).

Once these unknowns have been calculated, the EPC program determines the line-to-neutral voltages of the first load ( $\bar{V}_{AN1}$ ,  $\bar{V}_{BN1}$ ,  $\bar{V}_{CN1}$ ), of the second load ( $\bar{V}_{AN2}$ ,  $\bar{V}_{BN2}$ ,  $\bar{V}_{CN2}$ ), and of the source ( $\bar{V}_{AN'}$ ,  $\bar{V}_{BN'}$ ,  $\bar{V}_{CN'}$ ), as follows:

$$\begin{aligned}
\bar{V}_{AN1} &= \bar{V}_{AN} - \bar{V}_{N1N} \quad \bar{V}_{AN2} = \bar{V}_{AN} - \bar{V}_{N2N} \quad \bar{V}_{AN'} = \bar{V}_{AN} - \bar{V}_{N'N} \\
\bar{V}_{BN1} &= \bar{V}_{BN} - \bar{V}_{N1N} \quad \bar{V}_{BN2} = \bar{V}_{BN} - \bar{V}_{N2N} \quad \bar{V}_{BN'} = \bar{V}_{BN} - \bar{V}_{N'N} \\
\bar{V}_{CN1} &= \bar{V}_{CN} - \bar{V}_{N1N} \quad \bar{V}_{CN2} = \bar{V}_{CN} - \bar{V}_{N2N} \quad \bar{V}_{CN'} = \bar{V}_{CN} - \bar{V}_{N'N},
\end{aligned} \quad (9)$$

as well as the line-to-line voltages of these subsystems:

$$\begin{aligned}
\bar{V}_{AB1} &= \bar{V}_{AN1} - \bar{V}_{BN1} \quad \bar{V}_{AB2} = \bar{V}_{AN2} - \bar{V}_{BN2} \quad \bar{V}_{AB} = \bar{V}_{AN} - \bar{V}_{BN} \\
\bar{V}_{BC1} &= \bar{V}_{BN1} - \bar{V}_{CN1} \quad \bar{V}_{BC2} = \bar{V}_{BN2} - \bar{V}_{CN2} \quad \bar{V}_{BC} = \bar{V}_{BN} - \bar{V}_{CN} \\
\bar{V}_{CA1} &= \bar{V}_{CN1} - \bar{V}_{AN1} \quad \bar{V}_{CA2} = \bar{V}_{CN2} - \bar{V}_{AN2} \quad \bar{V}_{CA} = \bar{V}_{CN} - \bar{V}_{AN},
\end{aligned} \quad (10)$$

the line-to-neutral and line-to-line secondary voltages of the transformer:

$$\begin{aligned}
\bar{V}_{RN'} &= \bar{E}_a - \bar{Z}_{cc} \bar{I}_a \quad \bar{V}_{SN'} = \bar{E}_b - \bar{Z}_{cc} \bar{I}_b \quad \bar{V}_{TN'} = \bar{E}_c - \bar{Z}_{cc} \bar{I}_c \\
\bar{V}_{RS} &= \bar{V}_{RN} - \bar{V}_{SN} \quad \bar{V}_{ST} = \bar{V}_{SN} - \bar{V}_{TN} \quad \bar{V}_{TR} = \bar{V}_{TN} - \bar{V}_{RN},
\end{aligned} \quad (11)$$

the line, source, and transformer secondary currents:

$$\bar{I}_a = \frac{\bar{E}_a - \bar{V}_{AN'}}{\bar{Z}_{cc} - \bar{Z}_{LA}} \quad \bar{I}_b = \frac{\bar{E}_b - \bar{V}_{BN'}}{\bar{Z}_{cc} - \bar{Z}_{LB}} \quad \bar{I}_c = \frac{\bar{E}_c - \bar{V}_{CN'}}{\bar{Z}_{cc} - \bar{Z}_{LC}}, \quad (12)$$

the first load currents:

$$\bar{I}_{a1} = \frac{\bar{V}_{AN1}}{\bar{Z}_{A1} + \bar{Z}_{LA1}} \quad \bar{I}_{b1} = \frac{\bar{V}_{BN1}}{\bar{Z}_{B1} + \bar{Z}_{LB1}} \quad \bar{I}_{c1} = \frac{\bar{V}_{CN1}}{\bar{Z}_{C1} + \bar{Z}_{LC1}}, \quad (13)$$

the second load currents:

$$\bar{I}_{a2} = \frac{\bar{V}_{AN2}}{\bar{Z}_{A2} + \bar{Z}_{LA2}} \quad \bar{I}_{b2} = \frac{\bar{V}_{BN2}}{\bar{Z}_{B2} + \bar{Z}_{LB2}} \quad \bar{I}_{c2} = \frac{\bar{V}_{CN2}}{\bar{Z}_{C2} + \bar{Z}_{LC2}}, \quad (14)$$

and the neutral currents:

$$\bar{I}_{n1} = \frac{\bar{V}_{N1N}}{\bar{Z}_{n1}} \quad \bar{I}_{n2} = \frac{\bar{V}_{N2N}}{\bar{Z}_{n2}} \quad \bar{I}_n = -\frac{\bar{V}_{N'N}}{\bar{Z}_n}, \quad (15)$$

Likewise, the line-to-line voltages in each subsystem ( $k$ ) are obtained applying Kirchhoff's second law, that is:

$$\bar{V}_{ABk} = \bar{V}_{ANk} - \bar{V}_{BNk} \quad \bar{V}_{BCk} = \bar{V}_{BNk} - \bar{V}_{CNk} \quad \bar{V}_{CAk} = \bar{V}_{CNk} - \bar{V}_{ANk} \quad (16)$$

- (c) Calculation of the active and reactive powers of each subsystem in stage (16) of the programming module. Based on the phasors of the voltages and currents, obtained in the previous stage; the complex power; the active power; and the reactive power are obtained, using the following equations:

- on the first load,

$$\bar{S}_1 = \bar{V}_{AN1} \cdot \bar{I}_{a1}^* + \bar{V}_{BN1} \cdot \bar{I}_{b1}^* + \bar{V}_{CN1} \cdot \bar{I}_{c1}^* \quad P_1 = Re [\bar{S}_1] \quad Q_1 = Im [\bar{S}_1], \quad (17)$$

- on the second load,

$$\bar{S}_2 = \bar{V}_{AN2} \cdot \bar{I}_{a2}^* + \bar{V}_{BN2} \cdot \bar{I}_{b2}^* + \bar{V}_{CN2} \cdot \bar{I}_{c2}^* \quad P_2 = Re [\bar{S}_2] \quad Q_2 = Im [\bar{S}_2], \quad (18)$$

- on the point of common coupling (PCC),

$$\bar{S}_{PCC} = \bar{V}_{AN} \cdot \bar{I}_a^* + \bar{V}_{BN} \cdot \bar{I}_b^* + \bar{V}_{CN} \cdot \bar{I}_c^* \quad P_{PCC} = Re [\bar{S}_{PCC}] \quad Q_{PCC} = Im [\bar{S}_{PCC}], \quad (19)$$

- on the source,

$$\bar{S}_s = \bar{V}_{AN'} \cdot \bar{I}_a^* + \bar{V}_{BN'} \cdot \bar{I}_b^* + \bar{V}_{CN'} \cdot \bar{I}_c^* \quad P_s = Re [\bar{S}_s] \quad Q_s = Im [\bar{S}_s], \quad (20)$$

- on the secondary of the transformer,

$$\bar{S}_T = \bar{V}_{RN'} \cdot \bar{I}_a^* + \bar{V}_{SN'} \cdot \bar{I}_b^* + \bar{V}_{TN'} \cdot \bar{I}_c^* \quad P_T = Re [\bar{S}_T] \quad Q_T = Im [\bar{S}_T], \quad (21)$$

- (d) Symmetrical components of voltages and currents in stage (17) of the programming module. In this stage, the positive-, negative-, and zero-sequence components of the line-to-neutral voltages of each subsystem are obtained by application of Fortescue's theorem [24]:

- in the first load,

$$\bar{V}_{AN1+} = \frac{1}{3} (\bar{V}_{AN1} + a\bar{V}_{BN1} + a^2\bar{V}_{CN1}) \quad \bar{V}_{AN1-} = \frac{1}{3} (\bar{V}_{AN1} + a^2\bar{V}_{BN1} + a\bar{V}_{CN1}) \quad \bar{V}_{AN10} = \frac{1}{3} (\bar{V}_{AN1} + \bar{V}_{BN1} + \bar{V}_{CN1}), \quad (22)$$

- in the second load,

$$\bar{V}_{AN2+} = \frac{1}{3} (\bar{V}_{AN2} + a\bar{V}_{BN2} + a^2\bar{V}_{CN2}) \quad \bar{V}_{AN2-} = \frac{1}{3} (\bar{V}_{AN2} + a^2\bar{V}_{BN2} + a\bar{V}_{CN2}) \quad \bar{V}_{AN20} = \frac{1}{3} (\bar{V}_{AN2} + \bar{V}_{BN2} + \bar{V}_{CN2}), \quad (23)$$

- in the point of common coupling (PCC),

$$\bar{V}_{AN+} = \frac{1}{3} (\bar{V}_{AN} + a\bar{V}_{BN} + a^2\bar{V}_{CN}) \quad \bar{V}_{AN-} = \frac{1}{3} (\bar{V}_{AN} + a^2\bar{V}_{BN} + a\bar{V}_{CN}) \quad \bar{V}_{AN0} = \frac{1}{3} (\bar{V}_{AN} + \bar{V}_{BN} + \bar{V}_{CN}), \quad (24)$$

- in the source,

$$\bar{V}_{AN'+} = \frac{1}{3} (\bar{V}_{AN'} + a\bar{V}_{BN'} + a^2\bar{V}_{CN'}) \quad \bar{V}_{AN'-} = \frac{1}{3} (\bar{V}_{AN'} + a^2\bar{V}_{BN'} + a\bar{V}_{CN'}) \quad \bar{V}_{AN'0} = \frac{1}{3} (\bar{V}_{AN'} + \bar{V}_{BN'} + \bar{V}_{CN'}), \quad (25)$$

- in the secondary of the transformer,

$$\bar{V}_{RN'+} = \frac{1}{3} (\bar{V}_{RN'} + a\bar{V}_{SN'} + a^2\bar{V}_{TN'}) \quad \bar{V}_{RN'-} = \frac{1}{3} (\bar{V}_{RN'} + a^2\bar{V}_{SN'} + a\bar{V}_{TN'}) \quad \bar{V}_{RN'0} = \frac{1}{3} (\bar{V}_{RN'} + \bar{V}_{SN'} + \bar{V}_{TN'}), \quad (26)$$

as well as the positive-sequence currents corresponding to each phase of each subsystem (not of the currents corresponding to the three phases of each subsystem), that is:

- in the first load,

$$\bar{I}_{a1+} = \frac{1}{3} \bar{I}_{a1} \quad \bar{I}_{b1+} = \frac{1}{3} a \bar{I}_{b1} \quad \bar{I}_{c1+} = \frac{1}{3} a^2 \bar{I}_{c1}, \quad (27)$$

- in the second load,

$$\bar{I}_{a2+} = \frac{1}{3} \bar{I}_{a2} \bar{I}_{b2+} = \frac{1}{3} a \bar{I}_{b2} \bar{I}_{c2+} = \frac{1}{3} a^2 \bar{I}_{c2}, \quad (28)$$

- in the PCC, source and secondary of the transformer,

$$\bar{I}_{a+} = \frac{1}{3} \bar{I}_a \bar{I}_{b+} = \frac{1}{3} a \bar{I}_b \bar{I}_{c+} = \frac{1}{3} a^2 \bar{I}_c, \quad (29)$$

being  $a = 1 \angle 120^\circ$  and  $a^2 = 1 \angle 240^\circ$  in the previous equations.

(e) Calculation of the positive-sequence powers in stage (18) of the programming module. In this stage, the positive-sequence apparent, active, and reactive powers are calculated in each of the subsystems, as follows:

- in the first load,

$$\bar{S}_{1+} = \bar{V}_{AN1+} \cdot (\bar{I}_{a1+}^* + \bar{I}_{b1+}^* + \bar{I}_{c1+}^*) \quad P_{1+} = \text{Re} [\bar{S}_{1+}] \quad Q_{1+} = \text{Im} [\bar{S}_{1+}]$$

$$P_{A1+} = \text{Re} [\bar{V}_{AN1+} \cdot \bar{I}_{a1+}^*] \quad P_{B1+} = \text{Re} [\bar{V}_{AN1+} \cdot \bar{I}_{b1+}^*] \quad P_{C1+} = \text{Re} [\bar{V}_{AN1+} \cdot \bar{I}_{c1+}^*] \quad (30)$$

$$Q_{A1+} = \text{Im} [\bar{V}_{AN1+} \cdot \bar{I}_{a1+}^*] \quad Q_{B1+} = \text{Im} [\bar{V}_{AN1+} \cdot \bar{I}_{b1+}^*] \quad Q_{C1+} = \text{Im} [\bar{V}_{AN1+} \cdot \bar{I}_{c1+}^*],$$

- in the second load,

$$\bar{S}_{2+} = \bar{V}_{AN2+} \cdot (\bar{I}_{a2+}^* + \bar{I}_{b2+}^* + \bar{I}_{c2+}^*) \quad P_{2+} = \text{Re} [\bar{S}_{2+}] \quad Q_{2+} = \text{Im} [\bar{S}_{2+}]$$

$$P_{A2+} = \text{Re} [\bar{V}_{AN2+} \cdot \bar{I}_{a2+}^*] \quad P_{B2+} = \text{Re} [\bar{V}_{AN2+} \cdot \bar{I}_{b2+}^*] \quad P_{C2+} = \text{Re} [\bar{V}_{AN2+} \cdot \bar{I}_{c2+}^*] \quad (31)$$

$$Q_{A2+} = \text{Im} [\bar{V}_{AN2+} \cdot \bar{I}_{a2+}^*] \quad Q_{B2+} = \text{Im} [\bar{V}_{AN2+} \cdot \bar{I}_{b2+}^*] \quad Q_{C2+} = \text{Im} [\bar{V}_{AN2+} \cdot \bar{I}_{c2+}^*],$$

- in the point of common coupling (PCC),

$$\bar{S}_{PCC+} = \bar{V}_{AN+} \cdot (\bar{I}_{a+}^* + \bar{I}_{b+}^* + \bar{I}_{c+}^*) \quad P_{PCC+} = \text{Re} [\bar{S}_{PCC+}] \quad Q_{PCC+} = \text{Im} [\bar{S}_{PCC+}]$$

$$P_{PCC,A+} = \text{Re} [\bar{V}_{AN+} \cdot \bar{I}_{a+}^*] \quad P_{PCC,B+} = \text{Re} [\bar{V}_{AN+} \cdot \bar{I}_{b+}^*] \quad P_{PCC,C+} = \text{Re} [\bar{V}_{AN+} \cdot \bar{I}_{c+}^*] \quad (32)$$

$$Q_{PCC,A+} = \text{Im} [\bar{V}_{AN+} \cdot \bar{I}_{a+}^*] \quad Q_{PCC,B+} = \text{Im} [\bar{V}_{AN+} \cdot \bar{I}_{b+}^*] \quad Q_{PCC,C+} = \text{Im} [\bar{V}_{AN+} \cdot \bar{I}_{c+}^*],$$

- in the source,

$$\bar{S}_{s+} = \bar{V}_{AN'++} \cdot (\bar{I}_{a+}^* + \bar{I}_{b+}^* + \bar{I}_{c+}^*) \quad P_{s+} = \text{Re} [\bar{S}_{s+}] \quad Q_{s+} = \text{Im} [\bar{S}_{s+}]$$

$$P_{sA+} = \text{Re} [\bar{V}_{AN'++} \cdot \bar{I}_{a+}^*] \quad P_{sB+} = \text{Re} [\bar{V}_{AN'++} \cdot \bar{I}_{b+}^*] \quad P_{sC+} = \text{Re} [\bar{V}_{AN'++} \cdot \bar{I}_{c+}^*] \quad (33)$$

$$Q_{sA+} = \text{Im} [\bar{V}_{AN'++} \cdot \bar{I}_{a+}^*] \quad Q_{sB+} = \text{Im} [\bar{V}_{AN'++} \cdot \bar{I}_{b+}^*] \quad Q_{sC+} = \text{Im} [\bar{V}_{AN'++} \cdot \bar{I}_{c+}^*],$$

- in the secondary of the transformer,

$$\bar{S}_{T+} = \bar{V}_{RN'++} \cdot \bar{I}_{a+}^* + \bar{V}_{SN'++} \cdot \bar{I}_{b+}^* + \bar{V}_{TN'++} \cdot \bar{I}_{c+}^* \quad P_{T+} = \text{Re} [\bar{S}_{T+}] \quad Q_{T+} = \text{Im} [\bar{S}_{T+}]$$

$$P_{TR+} = \text{Re} [\bar{V}_{RN'++} \cdot \bar{I}_{a+}^*] \quad P_{TS+} = \text{Re} [\bar{V}_{SN'++} \cdot \bar{I}_{b+}^*] \quad P_{TT+} = \text{Re} [\bar{V}_{TN'++} \cdot \bar{I}_{c+}^*] \quad (34)$$

$$Q_{TR+} = \text{Im} \left[ \bar{V}_{RN'+} \cdot \bar{I}_{a+}^* \right] \quad Q_{TS+} = \text{Im} \left[ \bar{V}_{RN'+} \cdot \bar{I}_{b+}^* \right] \quad Q_{TT+} = \text{Im} \left[ \bar{V}_{RN'+} \cdot \bar{I}_{c+}^* \right]$$

- (f) Calculation of the unbalanced power vector and its components in stage (19) of the programming module. In this stage, the unbalanced power vector and its components are calculated in each of the subsystems, as indicated in reference [6], namely:

- unbalanced power vector and value of its norm in each subsystem ( $k$ ):

$$\vec{S}_{uk} = S_{uipk} \cdot \vec{p} + S_{uiqk} \cdot \vec{q} + S_{uvk} \cdot \vec{z} \quad S_{uk} = \sqrt{S_{uipk}^2 + S_{uiqk}^2 + S_{uvk}^2}, \quad (35)$$

- norm of the  $S_{uipk}$  component of  $\vec{S}_{uk}$ ,

$$S_{uipk} = \left| S_{uipk}^{\vec{}} \right| = \sqrt{2 \cdot (1 + G_{Uk}^2 + G_{Ak}^2)} \cdot |P_{A+k} + a^2 P_{B+k} + a P_{C+k}|, \quad (36)$$

which measures the effects of the active power imbalances in each subsystem ( $k$ ), where  $| \cdot |$  indicates the module of a phasor quantity in Gauss' plane and  $a = 1 \angle 120^\circ$ , and  $a^2 = 1 \angle 240^\circ$ .

- norm of the  $S_{uiqk}$  component of  $\vec{S}_{uk}$ ,

$$S_{uiqk} = \left| S_{uiqk}^{\vec{}} \right| = \sqrt{2 \cdot (1 + G_{Uk}^2 + G_{Ak}^2)} \cdot |\bar{Q}_{A+k} + a^2 \bar{Q}_{B+k} + a \bar{Q}_{C+k}|, \quad (37)$$

which measures the effects of the reactive power imbalances in each subsystem ( $k$ ).

- norm of the  $S_{uik}$  component of  $\vec{S}_{uk}$ ,

$$S_{uik} = S_{uipk} \cdot \vec{p} + S_{uiqk} \cdot \vec{q} \quad S_{uik} = \left| S_{uik}^{\vec{}} \right| = \sqrt{S_{uipk}^2 + S_{uiqk}^2} \quad (38)$$

which measures the combined effects of active and reactive power imbalances in each subsystem ( $k$ ),

- norm of the  $S_{uvk}$  component of  $\vec{S}_{uk}$ ,

$$S_{uvk} = \left| S_{uvk}^{\vec{}} \right| = \sqrt{G_{Uk}^2 + G_{Ak}^2} \cdot |\bar{S}_{+k}|, \quad (39)$$

which measures the effects of the unbalanced voltages in each subsystem ( $k$ ), being  $G_{Uk}$  and  $G_{Ak}$ ,

$$G_{Uk} = \frac{V_{-k}}{V_{+k}} \quad G_{Ak} = \frac{V_{0k}}{V_{+k}}, \quad (40)$$

the negative- and zero-sequence voltage degrees of each subsystem ( $k$ ).

- (g) Calculation of the norm ( $S_k$ ) of the apparent power vector in stage (20) of the programming module. In this stage, the apparent power vector is calculated at the fundamental-frequency in each subsystem ( $\vec{S}_k$ ), based on the values of its components: the positive-sequence active power ( $P_{+k}$ ); the positive-sequence reactive power ( $\bar{Q}_{+k}$ ); and the components of the unbalance power vector (obtained in step f), as follows:

$$\vec{S}_k = P_{+k} + \bar{Q}_{+k} + S_{uipk} \cdot \vec{p} + S_{uiqk} \cdot \vec{q} + S_{uvk} \cdot \vec{z} \quad S_k = \left| \vec{S}_k \right| = \sqrt{P_{+k}^2 + \bar{Q}_{+k}^2 + S_{uipk}^2 + S_{uiqk}^2 + S_{uvk}^2} \quad (41)$$

- (h) Calculation of the displacement power of the neutral in stage (21) of the programming module. In this stage, the value of the neutral-displacement power ( $S_{nk}$ ) and its relative value with the apparent power ( $S_{nk}/S_k$ ) are calculated, as follows:



- Neutral-displacement power of each subsystem ( $k$ ):

$$S_{nk} = \frac{\sqrt{3} V_{0k}}{\sum_z V_{zk}^2} \cdot S_k \quad (42)$$

where  $V_{0k}$  is the zero-sequence component of the simple stresses in subsystem  $k$ , calculated in step d, and  $\sum_z V_{zk}^2$  is the sum of the squares of the line-to-neutral voltages in each subsystem.

- Relative value of the neutral-displacement power in the subsystem  $k$ :

$$\frac{S_{nk}}{S_k} = \frac{\sqrt{3} V_{0k}}{\sum_z V_{zk}^2} \quad (43)$$

The value of this dimensionless parameter increases with the deterioration of the neutral conductor.

- (i) Calculation of the effective voltages and currents in stage (22) of the programming module. In this stage, the fundamental-frequency effective voltages and currents ( $V_e$ ,  $I_e$ ) are calculated in the PCC, according to the IEEE Standard 1459-2010, as follows:

$$V_e = \sqrt{\frac{1}{9 \cdot (1 + \xi)} [3 \cdot (V_{AN}^2 + V_{BN}^2 + V_{CN}^2) + \xi \cdot (V_{AB}^2 + V_{BC}^2 + V_{CA}^2)]} \quad (44)$$

$$I_e = \sqrt{\frac{1}{3} (I_a^2 + I_b^2 + I_c^2 + \rho I_n^2)} \quad (45)$$

where the parameters

$$\xi = \frac{P_\Delta}{P_Y} \quad \rho = \frac{r_n}{r} \quad (46)$$

are the ratios between the active power consumed in the system by the delta ( $P_\Delta$ ) and star ( $P_Y$ ) loads and between the resistance of the neutral ( $r_n$ ) and of the lines ( $r$ ), respectively. In case the values of  $P_\Delta$  and  $P_Y$  are not known, the IEEE 1459-2010 standard suggests using the value  $\xi = 1$ . However, in the circuit of Figure 1,  $\xi = 0$ , since there are no delta loads.

- (j) Calculation of the effective apparent power in stage (23) of the programming module. In this stage, the values of the fundamental-frequency effective apparent power are obtained, in the PCC, according to IEEE 1459-2010 standard, as follows:

$$S_e = 3 \cdot V_e \cdot I_e \quad (47)$$

- (k) Calculation of the apparent power according to DIN 40110-2 in stage (24) of the programming module. In this stage, the values of the fundamental-frequency apparent power are obtained in the PCC, according to DIN 40110-2, as follows:

$$S_{DIN} = \sqrt{\frac{1}{4} (V_{AN}^2 + V_{BN}^2 + V_{CN}^2 + V_{AB}^2 + V_{BC}^2 + V_{CA}^2) \cdot (I_a^2 + I_b^2 + I_c^2 + I_n^2)} \quad (48)$$

- (l) The values obtained in the previous steps are displayed on the “apparent power and components” screen in stage (25) of the programming module, as shown in Figure 3.

### 3.2.2. Voltage and Current Programming Module

This programming module consists of three stages (Figure 7) and is responsible for collecting the values of voltages and currents in the phases of each subsystem ( $k$ ), obtained in stage (15) of the programming module, according to the equations expressed in step b. The values of voltages and currents are displayed in tables on the “system voltage and current” screen (Figure 5) in the programming module (26).

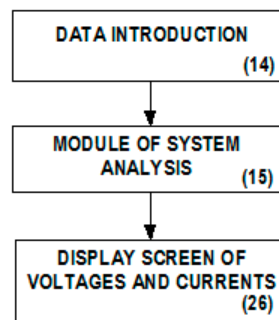


Figure 7. Voltage and current programming module.

#### 4. Practical Validation

The correctness of the results calculated with the EPC software is verified in a practical case in this section. The values of voltages, currents, and powers calculated with the EPC software were compared to those measured with the Fluke 435 Series II analyzer in the PCC of one of the transformation houses of the actual low-voltage distribution network that supplies apartment buildings (Figure 8). Alike, the values of voltages and currents calculated by the EPC were compared to those obtained at the point of common coupling with those obtained using the Multisim commercial software (Figure 9).

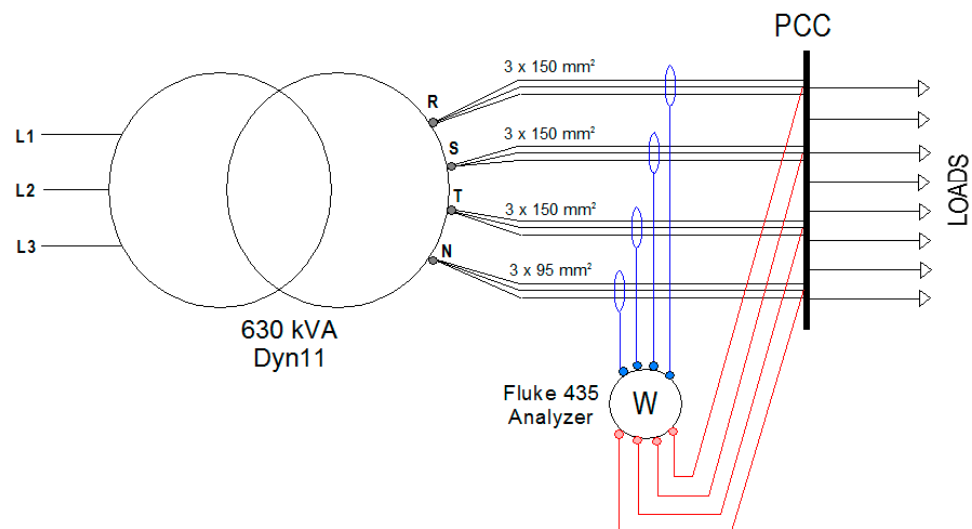


Figure 8. Scheme of the actual residential distribution network used in the application example and placement of the Fluke 435 Series II analyzer.

The transformer was delta wye, had a nominal power of 630 kVA, and could be connected to the 24 kV electrical network. Its no-load secondary voltage was regulated at 395 V. The short-circuit voltage was 4%, the no-load losses were 1300 W, and the copper losses were 6500 W (Figure 10a).

To simplify the study, we grouped all the loads connected to the PCC (Figure 8) in only one equivalent load, as show in Figure 9. Thevenin's impedances of this equivalent load, including its lines, were obtained by the quotient between the line-to-neutral voltages and the line currents measured by the Fluke 435 analyzer, in each phase of the PCC (Figure 8). Their values were  $\bar{Z}_A = 2.3126 \angle -3.1^\circ$ ,  $\bar{Z}_B = 2.2728 \angle -1.9^\circ$ ,  $\bar{Z}_C = 1.9873 \angle -9.2^\circ$ , at the instance the Fluke 435 analyzer measured voltages and currents (11:57:58, 01/12/22, Figure 11a). These values were entered in the "system data" screen of the EPC (Figure 10d).

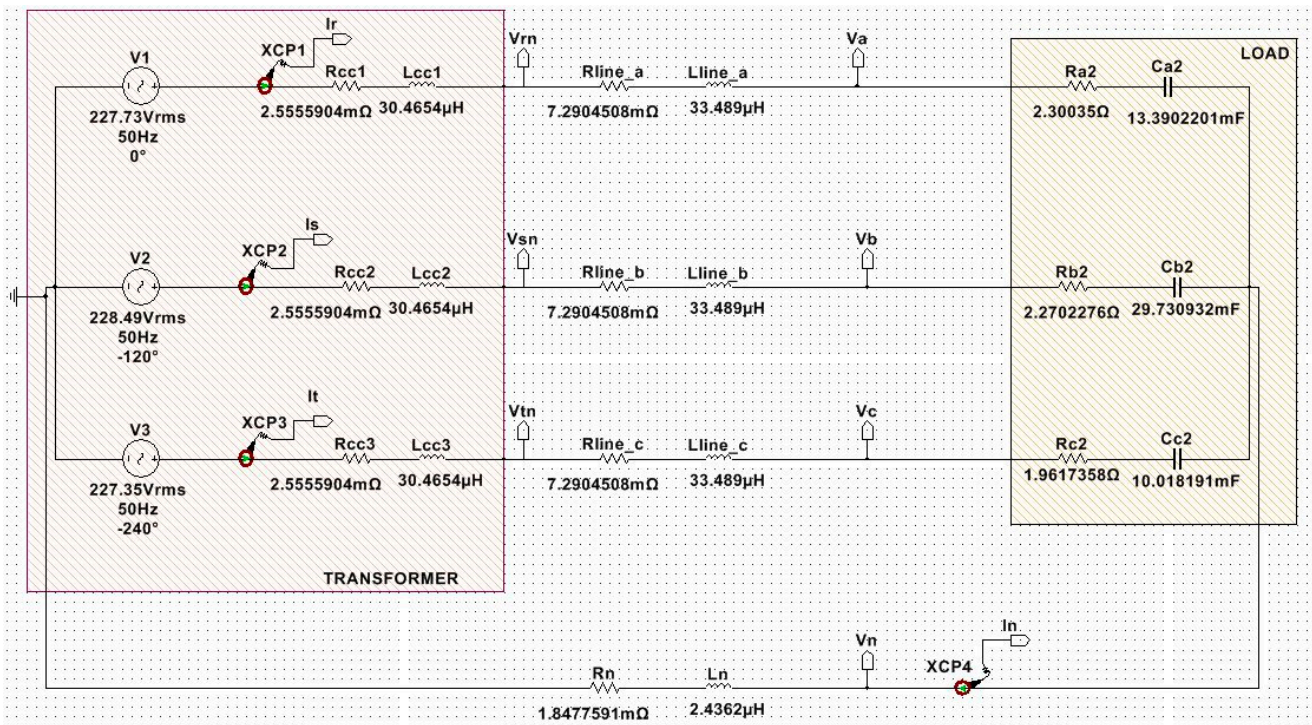


Figure 9. Simulation scheme of the distribution network using Multisim software.

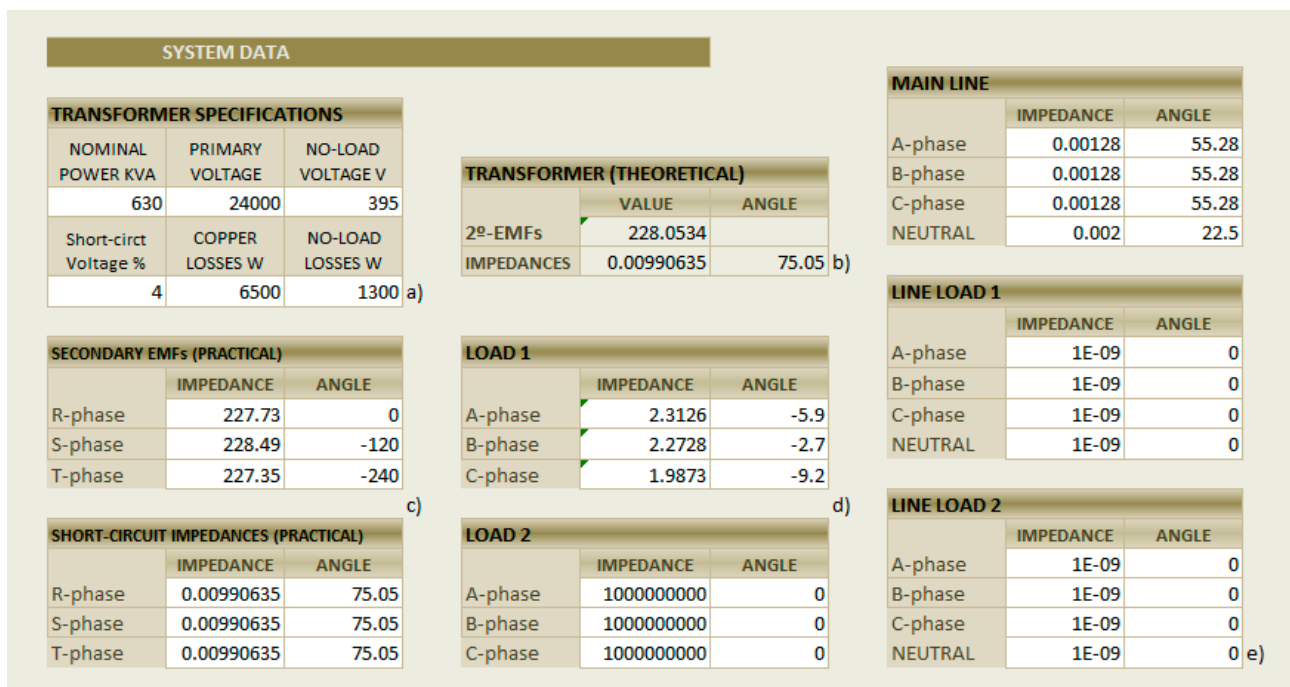
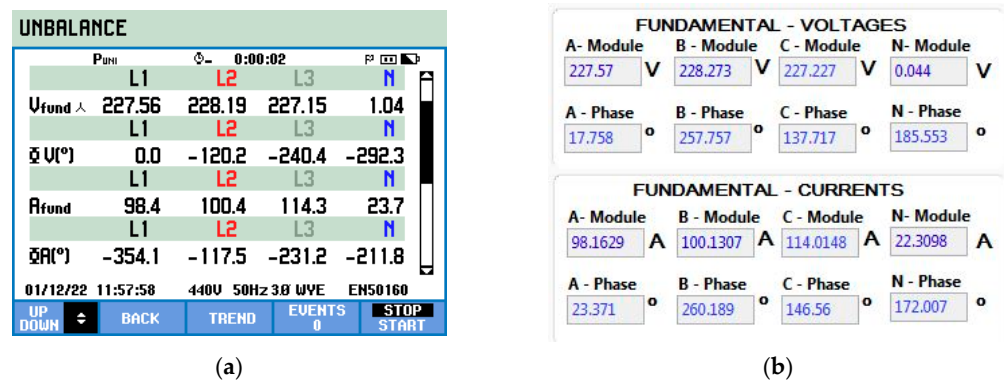


Figure 10. “System data” screen after entering transformer, line, and load data; (a) transformer features; (b) theoretical values of transformer secondary EMFs and short-circuit impedances; (c) practical values of secondary EMFs and short-circuit impedances; (d) load impedances; and (e) line and neutral conductor impedances.



**Figure 11.** Complex RMS values of the line-to-neutral voltages and line currents: (a) measured by the Fluke 435 analyzer, and (b) calculated by Multisim, using LabVIEW.

The main lines between the transformer and the PCC were 4 m long and were made up of three conductors with a section of 150 mm<sup>2</sup>, in each phase. This resulted in a complex impedance of 0.00128∠55.28° per phase. The neutral conductor comprised three conductors with a section of 90 mm<sup>2</sup>, with a total complex impedance of 0.002∠22.5° (Figure 10e).

#### 4.1. Validation of Voltages and Currents Calculated by the EPC Software

The values of the voltages and currents obtained by the EPC software are compared in this section with those measured by the Fluke 435 analyzer in the PCC of the distribution network (Figure 11a) and calculated using the Multisim commercial software (Figure 11b).

Once the nominal values of the transformer (Figure 10a), loads (Figure 10d), and lines (Figure 10e) were entered on the “system data” screen, the EPC software provided the theoretical values of the secondary Electromotive Forces (EMFs) and short-circuit impedances of the transformer (Figure 10b). However, entering these latter values directly into the tables in Figure 10c EPC did not provide the same voltage and current values recorded by the Fluke 435 Series II analyzer. This fact can be explained by the fact that the transformer has a small asymmetry and its EMFs are not balanced, in practice. For this reason, the first step was to adjust the EMF values in the tables of Figure 10c until the EPC software gave us the same RMS voltage values as those measured by the Fluke analyzer at the PCC (Figure 11a). The validity of the adjustment made to the transformer EMFs on the EPC software was demonstrated by the fact that the line currents calculated by the EPC software (Figure 12) provided the same RMS values as those recorded by the Fluke 435 analyzer (Figure 11a) for those values of the transformer EMFs. Thus, the relative difference of 5.5% between the RMS neutral currents measured by the Fluke analyzer and calculated by the EPC software must be attributed to an error in the Fluke’s measurement, caused by the small value of the neutral current compared to the caliber of the Fluke’s current sensor (note that the neutral current was much less than the line currents, Figure 11a).

		A - phase	B - phase	C - phase	Neutral
line-N	RMS	227.56	228.19	227.15	
	ANGLE	-0.27	-120.26	119.67	
line-line	RMS	394.67	394.46	393.67	
	ANGLE	29.78	-90.37	149.73	
CURRENTS	RMS	98.40	100.40	114.30	22.44
	ANGLE	5.63	-117.56	128.87	154.58

**Figure 12.** Voltages and currents calculated by the EPC software at the point of common coupling (PCC) of the residential distribution network.

Comparing the values of voltages and currents calculated through the EPC software (Figure 12) and obtained by Multisim (Figure 11b), slight differences were observed of less

than 0.037% in voltages and 0.58% in currents. However, the values obtained with the EPC software were closer to the actual values measured with the Fluke 435 analyzer.

4.2. Validation of Powers Calculated by the EPC Software

The apparent powers and their components calculated using the EPC software at the PCC were compared, at the industrial frequency, with those recorded by the Fluke 435 Series II analyzer, using two options: (1) according to Fluke’s unified power measurement (UNI) (Figure 13a), and (2) according to the IEEE 1459-2010 standard (Figure 13b). Unlike the EPC software, the Fluke 435 analyzer does not have the option to measure the apparent power value according to DIN 40110-2.

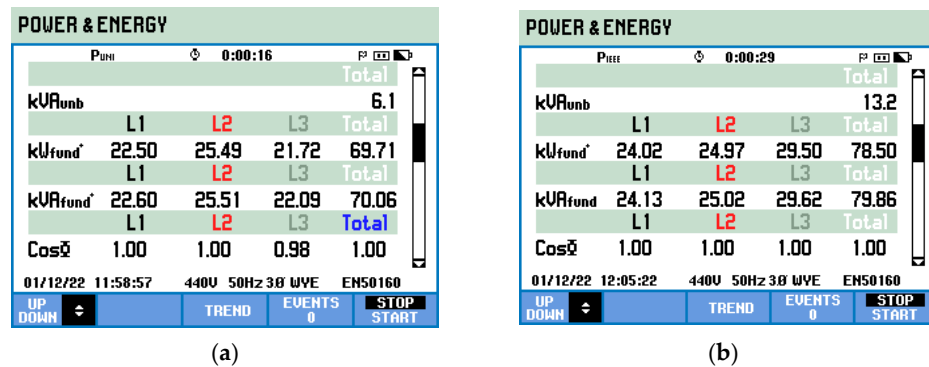


Figure 13. Fluke’s power screens for the PCC of the residential distribution network according to: (a) Fluke’s unified power measurement ( $P_{UNI}$ ) and (b) IEEE 1459 ( $P_{IEEE}$ ) standard.

The screens of the Fluke 435 Series II analyzer do not provide the values of all the powers it measures. This fact can be seen, for example, in Fluke’s power screen, according to UNI (Figure 13a), in which only the values of unbalanced power ( $kVA_{unb}$ ), fundamental-frequency positive-sequence active power ( $kW_{fund+}$ ), and fundamental-frequency positive-sequence apparent power are indicated. Fluke’s power screen, according to IEEE (Figure 13b), only shows the values of the unbalanced power ( $kVA_{unb}$ ), the fundamental-frequency positive-sequence active power ( $kW_{fund+}$ ), and the fundamental-frequency apparent power ( $kVA_{fund}$ ). Therefore, the comparison with the powers calculated by the EPC software (Figure 14) was made based on these powers only (Table 1).

POINT OF COMMON COUPLING (PCC)					
APPARENT POWERS AND COMPONENTS					
	S	P+	Q+	S+	S <sub>u</sub>
VALUE	71434.08	70793.70	-7536.523	71193.73	5854.96
VALUE	P	Q			
	70785.95	-7531.8			
UNBALANCED POWER AND COMPONENTS (VA)					
	S <sub>uip</sub>	S <sub>uiq</sub>	S <sub>ui</sub>	S <sub>uv</sub>	S <sub>u</sub>
VALUE	4480.50	3766.48	5853.31	138.78	5854.96
NEUTRAL - DISPLACEMENT POWER					
	S <sub>n</sub> (VA)	S <sub>n</sub> /S			
VALUE	85.61	0.0012			
IEEE 1459 & DIN 40110 POWERS					
PCC APPARENT AND UNBALANCED POWERS					
STANDARD	APPARENT POWER (VA)				
IEEE 1459 ( $\xi=1$ )	72284.77				
IEEE 1459 ( $\xi=P\Delta/PY$ )	72284.80				
DIN 40110-2	71979.66				

Figure 14. Apparent ( $\vec{S}$ ) and unbalanced ( $\vec{S}_u$ ) power vectors, neutral-displacement power ( $S_n$ ), and IEEE-1459 and DIN-40110 standards apparent powers calculated by the EPC software in the PCC.



**Table 1.** Summary of powers calculated by the EPC software and measured by the Fluke 435 Series II analyzer and their comparison. (\*) determined according to  $S_{u, IEEE} = \sqrt{S_{IEEE}^2 - S_{+}^2}$ .

UNI				IEEE			
POWER	EPC	Fluke	Difference (%)	POWER	EPC	Fluke	Difference (%)
$S_{+}$ (kVA) (kVAfund <sup>+</sup> )	71.19	70.06	1.59	$S$ (kVA) (kVAfund)	72.28	79.86	−10.49
$P_{+}$ (kW) (kWfund <sup>+</sup> )	70.79	69.71	1.52	$P_{+}$ (kW) (kWfund <sup>+</sup> )	70.79	78.50	−10.89
$S_u$ (kVA) (kVAunb)	5.85	6.10	−4.27	$S_u$ (kVA) (kVAunb)	12.51 *	13.20	−5.51

From Table 1, some differences between powers calculated by the EPC software and measured by the Fluke 435 Series II analyzer were noted. Fluke’s measuring powers were lower according to UNI than according to the IEEE 1459 standard. Power differences must be attributed to the fact that all the EPC power calculations were made for the same instance in which the Fluke analyzer measured the voltages and currents (11:57:58, Figure 11a). However, the power measurements with the Fluke analyzer were made at different times compared to the voltage and current measurements. This is because it was necessary to carry out operations on the analyzer in order to change from the voltage and current measurement to power measurement, and even to change from the UNI to the IEEE. Indeed, Fluke’s power measurements were carried out, according to the UNI, at 11:58:57 (Figure 13a). This occurred almost one minute after the measurement of voltages and currents, when the operating conditions of the network of distribution had not varied much. However, Fluke’s power measurements were made, according to IEEE, at 12:05:22 (Figure 13b), i.e., more than six minutes after the measurement of voltages and currents, when the operating conditions of the distribution network had changed significantly.

## 5. Conclusions

The EPC software for the simulation and analysis of three-phase sinusoidal networks, among which many distribution networks of residential buildings can be included, has been extensively described in this article. Evenly, its correct operation has been verified comparing the results of its analysis using the Multisim commercial software and the measurements recorded by the Fluke 435 Series II analyzer in a real distribution network, which supplies apartment buildings.

The comparison of the values of voltages and currents calculated by the EPC software and obtained by the Multisim commercial software determined small differences of less than 0.037% in voltages and 0.58% in currents. In addition, there were no differences between the values of voltages and currents calculated by the EPC software and those measured by the Fluke 435 analyzer in the PCC of the distribution network of the residential buildings supplied.

The power values calculated by the EPC software have been compared with those recorded by the Fluke 435 analyzer, according to two electrical power theories: the unified power measurement (UNI), sponsored by Fluke, and that sponsored by the IEEE 1459-2010 standard. A problem with comparing the power values has arisen from the fact that the EPC software calculates the powers at the same instance as the voltages and currents. However, the powers measured by the Fluke 435 analyzer, which requires time spent in operations to change the measured quantities, are carried out at different times. As a result of the operations required, the power measurement with the Fluke 435 analyzer was carried out when there had been changes in the loads of the distribution network. Despite this, it has been verified that powers calculated by the EPC in vector notation provide values very close to those measured by the Fluke 435 analyzer almost one minute later, according to UNI. However, the power differences according to the IEEE were almost 11% higher as more than 6 min had elapsed between measurements.

Another EPC software application that, in our opinion, may be of interest to users and manufacturers of measuring instruments is to complement the features of commercial network analyzers, by either:

1. Measuring powers according to theories not available in the analyzer, or
2. Analyzing the operation of all the subsystems of the distribution network using only one analyzer at the same time.

This second application of the EPC software has allowed the detection of the presence of transformer structural asymmetries in the actual distribution network of apartment buildings used as a practical application in this paper.

## 6. Patents

The following patents and intellectual property have resulted from the work reported in this manuscript:

- Vicente León-Martínez and Joaquín Montañana-Romeu. Method and system for measuring imbalances in an electrical grid. Spanish patent ES2544902B2. Granted 22 December 2015.
- Vicente León-Martínez and Joaquín Montañana-Romeu. Procedure and device for the determination of the state of the neutral conductor in an electrical installation Spanish patent ES2588260B2. Granted 28 April 2017.
- Vicente León-Martínez, Joaquín Montañana-Romeu, and Elisa Peñalvo López. Electric Power Calculator: Software for calculating apparent power and its components in power systems. Registered software of the Universitat Politècnica de València. Registration date: 29 April 2022.

**Author Contributions:** Conceptualization, V.L.-M., J.M.-R. and E.P.-L.; methodology, V.L.-M., J.M.-R. and E.P.-L.; software, V.L.-M., J.M.-R. and E.P.-L.; validation, V.L.-M., J.M.-R., E.P.-L., M.A.G.-L. and I.V.-S.; formal analysis, V.L.-M., J.M.-R., E.P.-L., M.A.G.-L. and I.V.-S.; investigation, V.L.-M., J.M.-R., M.A.G.-L. and I.V.-S.; resources, V.L.-M., J.M.-R., E.P.-L. and I.V.-S.; data curation, V.L.-M. and J.M.-R.; writing—original draft preparation, V.L.-M., M.A.G.-L. and I.V.-S.; writing—review and editing, V.L.-M., M.A.G.-L. and I.V.-S.; visualization, V.L.-M., E.P.-L. and M.A.G.-L.; supervision, V.L.-M., J.M.-R. and M.A.G.-L.; project administration, V.L.-M., E.P.-L. and I.V.-S.; funding acquisition, E.P.-L. All authors have read and agreed to the published version of the manuscript.

**Funding:** This research was funded by Generalitat Valenciana, grant number GV/2021/149.

**Acknowledgments:** We kindly appreciate the support provided by the company Eléctrica de Vinalosa, S.C.V., by allowing us access to its distribution networks, as well as the economic funding given by the Generalitat Valenciana.

**Conflicts of Interest:** The authors declare no conflict of interest.

## References

1. Multisim. User Manual. *National Instruments*. Available online: <https://www.ni.com/docs/en-US/search?q=NI%20Multisim%20User%20Manual> (accessed on 2 December 2022).
2. LTSpice. Analog Devices. Available online: <https://www.analog.com/en/design-center/design-tools-and-calculators/ltspice-simulator.html> (accessed on 2 December 2022).
3. Proteus. PCB Design Software. Available online: <https://www.labcenter.com/pcb/> (accessed on 2 December 2022).
4. PSCAD. Manitoba Hydro International Ltd. Available online: <https://www.pscad.com/software/pscad/overview> (accessed on 2 December 2022).
5. León-Martínez, V.; Montañana-Romeu, J. Formulations for the apparent and unbalanced power vectors in three-phase sinusoidal systems. *Electr. Power Syst. Res.* **2018**, *160*, 37–43. [CrossRef]
6. Buchholz, F. Die drehstrom-scheinleistung bei ungleichmassiger belastungder drei zweige. *Licht Kraft* **1922**, *2*, 9–11.
7. Abd-El-Hakeem Mohamed, M.; Ali, Z.M.; Ahmed, M.; Al-Gahtani, S.F. Energy saving maximization of balanced and unbalanced distribution power systems via network reconfiguration and optimum capacitor allocation using a hybrid metaheuristic algorithm. *Energies* **2021**, *14*, 3205. [CrossRef]
8. Dadashzade, A.; Aminifar, F.; Davarpanah, M. Unbalanced source detection in power distribution networks by negative sequence apparent powers. *IEEE Trans. Power Deliv.* **2021**, *36*, 481–483. [CrossRef]

9. Pratama, N.A.; Rahmawati, Y. Evaluation of unbalanced load impacts on distribution transformer performances. *Front. Energy Syst. Power Eng.* **2020**, *2*, 28–35. [[CrossRef](#)]
10. Gandluru, A.; Poudel, S.; Dubey, A. Joint estimation of operational topology and outages for unbalanced power distribution systems. *IEEE Trans. Power Syst.* **2020**, *35*, 205–217. [[CrossRef](#)]
11. Kettner, A.M.; Paolone, M. A generalized index for static voltage stability of unbalanced polyphase power systems including Thévenin equivalents and polynomial models. *IEEE Trans. Power Syst.* **2019**, *34*, 4630–4639. [[CrossRef](#)]
12. Abello, A.J. Power Measurement Model Optimization using MATLAB. *Int. J. Adv. Trends Comput. Sci. Eng.* **2019**, *8*, 538–543. [[CrossRef](#)]
13. Shakerighadi, B.; Aminifar, F.; Afsharnia, S. Power systems wide-area voltage stability assessment considering dissimilar load variations and credible contingencies. *J. Mod. Power Syst. Clean Energy* **2019**, *7*, 78–87. [[CrossRef](#)]
14. Nguyen, Q.; Padullaparti, H.V.; Lao, K.W.; Santoso, S.; Ke, X.; Samaan, N. Exact optimal power dispatch in unbalanced distribution systems with high PV penetration. *IEEE Trans. Power Syst.* **2019**, *34*, 718–728. [[CrossRef](#)]
15. Yan, S.; Wang, M.H.; Yang, T.B.; Tan, S.C. Achieving multiple functions of three-phase electric springs in unbalanced three-phase power systems using the instantaneous power theory. *IEEE Trans. Power Electron.* **2018**, *33*, 5784–5895. [[CrossRef](#)]
16. Xia, Y.; Kanna, S.; Mandic, D.P. Maximum likelihood parameter estimation of unbalanced three-phase power signals. *IEEE Trans. Instrum. Meas.* **2018**, *67*, 569–581. [[CrossRef](#)]
17. Sun, Y.; Xie, X.; Li, P. Unbalanced source identification at the point of evaluation in the distribution power systems. *Int. Trans. Electr. Energy Syst.* **2018**, *28*, e2460. [[CrossRef](#)]
18. Albadi, M.H.; Al Hinai, A.S.; Al-Badi, A.H.; Al Riyami, M.S.; Al Hinai, S.M.; Al Abri, R.S. Unbalance in power systems: Case study. In Proceedings of the IEEE International Conference on Industrial Technology (ICIT), Seville, Spain, 17–19 March 2015; pp. 1407–1411. [[CrossRef](#)]
19. Herrera, R.S.; Vázquez, J.R. Identification of unbalanced loads in electric power systems. *Int. Trans. Electr. Energy Syst.* **2014**, *24*, 1232–1243. [[CrossRef](#)]
20. Seiphethlo, T.E.; Rens, A.P.J. On the assessment of voltage unbalance. In Proceedings of the 14th International Conference on Harmonics and Quality of Power—ICHQP 2010, Bergamo, Italy, 26–29 September 2010. [[CrossRef](#)]
21. Leon-Martinez, V.; Montanana-Romeu, J.; Peñalvo-López, E.; Valencia-Salazar, I. Relationship between Buchholz’s Apparent Power and Instantaneous Power in Three-Phase Systems. *Appl. Sci.* **2020**, *10*, 1798. [[CrossRef](#)]
22. *IEEE Standard 1459-2010*; IEEE Trial-Use Standard for the Measurement of Electric Power Quantities Under Sinusoidal, Nonsinusoidal, Balanced or Unbalanced Conditions. IEEE: New York, NY, USA, 2010.
23. *DIN 40110*; Teil 2. Mehrleiter-Stromkreise. Beuth-Verlag: Berlin, Germany, 2002.
24. Fortescue, C.L. Method of symmetrical coordinates applied to solution of poly-phase networks. *Trans. Am. Inst. Electr. Eng.* **1918**, *37*, 1027–1140. [[CrossRef](#)]

**Disclaimer/Publisher’s Note:** The statements, opinions and data contained in all publications are solely those of the individual author(s) and contributor(s) and not of MDPI and/or the editor(s). MDPI and/or the editor(s) disclaim responsibility for any injury to people or property resulting from any ideas, methods, instructions or products referred to in the content.